

# Strongly enhanced local electromagnetic field in mid-infrared and terahertz photodetectors employing a hybrid antenna

Cite as: AIP Advances **10**, 015048 (2020); <https://doi.org/10.1063/1.5128270>

Submitted: 19 September 2019 . Accepted: 06 January 2020 . Published Online: 22 January 2020

Yuqing Cheng , Yan Xie, Zhixuan Wang, Yinshu Wang, Lianhe Li, Ning Yang , Suqing Duan, Yingxin Wang, Ziran Zhao, Jialin Sun, and Weidong Chu 



View Online



Export Citation



CrossMark

## ARTICLES YOU MAY BE INTERESTED IN

[High-responsivity and polarization-discriminating terahertz photodetector based on plasmonic resonance](#)

Applied Physics Letters **114**, 091105 (2019); <https://doi.org/10.1063/1.5085813>

[Enhanced terahertz absorption of quantum wells sandwiched between heavily doped contacts based on micro-cavity resonance](#)

Journal of Applied Physics **127**, 053104 (2020); <https://doi.org/10.1063/1.5131803>

[Ultra-broadband mid-infrared Ge-on-Si waveguide polarization rotator](#)

APL Photonics **5**, 026102 (2020); <https://doi.org/10.1063/1.5134973>



**NEW**

## AVS Quantum Science

A new interdisciplinary home for impactful quantum science research and reviews

Co-Published by



**NOW ONLINE**

# Strongly enhanced local electromagnetic field in mid-infrared and terahertz photodetectors employing a hybrid antenna

Cite as: AIP Advances 10, 015048 (2020); doi: 10.1063/1.5128270

Submitted: 19 September 2019 • Accepted: 6 January 2020 •

Published Online: 22 January 2020



Yuqing Cheng,<sup>1</sup> Yan Xie,<sup>2</sup> Zhixuan Wang,<sup>1,3</sup> Yinshu Wang,<sup>3</sup> Lianhe Li,<sup>4</sup> Ning Yang,<sup>1,a)</sup> Suqing Duan,<sup>1</sup> Yingxin Wang,<sup>2</sup> Ziran Zhao,<sup>2</sup> Jialin Sun,<sup>5</sup> and Weidong Chu<sup>1,a)</sup>

## AFFILIATIONS

<sup>1</sup>Institute of Applied Physics and Computational Mathematics, Beijing 100088, China

<sup>2</sup>Department of Engineering Physics, Tsinghua University, Beijing 100084, China

<sup>3</sup>Department of Physics, Beijing Normal University, Beijing 100875, China

<sup>4</sup>School of Electronic and Electrical Engineering, University of Leeds, Leeds LS2 9JT, United Kingdom

<sup>5</sup>Department of Physics, Tsinghua University, Beijing 100084, China

<sup>a)</sup> Authors to whom correspondence should be addressed: [chu\\_weidong@iapcm.ac.cn](mailto:chu_weidong@iapcm.ac.cn) and [yang\\_ning@iapcm.ac.cn](mailto:yang_ning@iapcm.ac.cn)

## ABSTRACT

A hybrid antenna consisting of a patch cavity and a metal grating is designed in this work. This antenna can effectively localize and enhance the intensity of the electric field inside a quantum well photodetector (QWP). The optical properties of the designed antenna are theoretically investigated, and it is found that the electric field can be increased by a factor of  $\sim 10^4$  in the infrared region (6–10  $\mu\text{m}$ ) and  $\sim 10^5$  in the terahertz (THz) region (100  $\mu\text{m}$ ). These enhancements can greatly improve the performance of QWPs. In the THz region, it is theoretically estimated that the hybrid antenna can increase the working temperature of the detector to 195 K, and the noise equivalent power is theoretically estimated to be as low as  $\sim 10^{-18}$  W/Hz<sup>0.5</sup> at  $T = 4$  K and  $\sim 10^{-15}$  W/Hz<sup>0.5</sup> at room temperature,  $T = 300$  K. These results are of great significance for applications of QWPs.

© 2020 Author(s). All article content, except where otherwise noted, is licensed under a Creative Commons Attribution (CC BY) license (<http://creativecommons.org/licenses/by/4.0/>). <https://doi.org/10.1063/1.5128270>

## I. INTRODUCTION

Metamaterials have been widely investigated due to their excellent ability to control light at subwavelength scales.<sup>1–5</sup> In particular, the localized surface plasmon resonance (LSPR) modes supported within metamaterials can strongly enhance and localize the electromagnetic field, giving rise to a wide range of applications, such as high-resolution imaging, sensors, optical waveguides, optoelectronics technology, and quantum well infrared photodetectors (QWIPs).<sup>6–11</sup> QWIPs have been demonstrated as sensitive devices suitable for a variety of frequency ranges over the last three decades.<sup>12,13</sup> QWIPs are of great interest and have been widely used in thermal imaging, night vision, target detection, etc.<sup>14–16</sup> However, challenges remain in the application of QWIPs. For example, the signal to noise ratio (SNR) of QWIPs is still low at room

temperature due to the thermally induced dark current, particularly in the long-wave infrared region.<sup>17–19</sup> Researchers have expended substantial effort to solve this problem by employing different methods, including the use of metamaterials.

Recently, researchers<sup>10</sup> have employed a photonic metamaterial to increase the SNR in QWIPs and have demonstrated that their detector can operate at room temperature with high sensitivity at wavelengths of 8–12  $\mu\text{m}$ . In this work, we investigate a metamaterial, i.e., a hybrid antenna composed of a patch cavity and a metal grating, that can strongly enhance and localize the electric field inside the cavity. We apply our antenna to a QWIP and demonstrate that the intensity of the electric field inside the quantum well (QW) is greatly increased, thus resulting in a highly enhanced SNR and responsivity of the detector. With this antenna, the working temperature of the detector can be increased, with a potential for room temperature

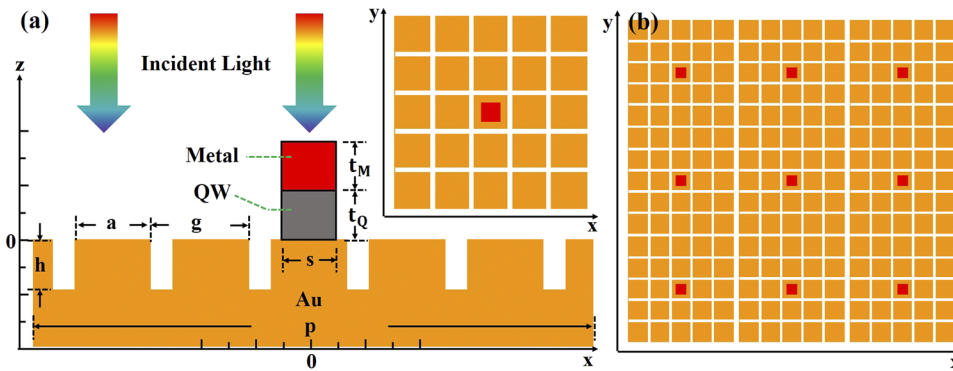


**FIG. 1.** Schematic of the hybrid antenna: (a) the unit cell from the x-z plane view; the inset shows the unit cell from the x-y plane view and (b) an x-y plane view of a 3 × 3 antenna; the red and gray patches are metal (Pd or Au) and QWs, respectively, where s is the patch size, and  $t_M$  and  $t_Q$  are the thicknesses of the metal and the QW, respectively. The yellow substrate is gold, which is etched into a grating with depth h, width a, and grating period g. The period of the unit cell is p.

detection. In addition, the working wavelength (or resonance wavelength) varies with the structure size, ranging from the infrared to terahertz (THz) region.

**II. METHODS**

The metamaterial proposed in this work consists of a patch cavity and a metal grating arranged in a periodic array. A schematic of our hybrid antenna is shown in Fig. 1, where Fig. 1(a) presents an x-z plane view of the unit cell and the inset of (a) presents an x-y plane image. Figure 1(b) presents an x-y plane view of a 3 × 3 antenna. A plane wave polarized along the x axis is chosen to illuminate the structure from above. The metal-dielectric-metal structure forms a patch cavity, also known as a patch resonator. Here, the top metal (red) is palladium (Pd) or gold (Au),<sup>20</sup> where both metals have the same effect, and the QW is GaAs<sup>21</sup> in this study. The gold substrate is etched into a grating. We investigate the properties (electric field enhancement) of the antenna by varying and optimizing parameters such as the size and period.

The patch resonator works as a cavity and enhances the intensity of the electric field inside the QW, while the patch array helps concentrate more photons due to the coupling effect among these patches.<sup>10</sup> Grating structures have been used to improve the electric field enhancement of photodetectors due to the coherent effect of gratings.<sup>22</sup> As a result, the responsivity R of the detector will be greatly increased. In Sec. III, we analyze the properties of our hybrid antenna in detail.

**III. RESULTS**

First, we briefly discuss the properties of a solitary patch antenna array (a patch antenna array without gratings). As previously reported,<sup>10</sup> the minimum of the reflectivity spectra, which indirectly represents the absorption cross section, varies with the array period p. In our study, we employ the electric field enhancement to represent the absorption ability of the structure. We define the enhancement factor as  $F = \frac{|E|^2}{|E_0|^2} = \frac{1}{V} \int |E_Q|^2 dV$ , where  $E_Q$  is the intensity of the electric field inside the QW,  $E_0$  is the intensity within the same volume in vacuum (no structures), and V is the volume of the QW. The integral is performed over the volume of the QW. Evidently, the factor F equals 1 in vacuum, and the responsivity  $R \propto F$  due to the relation between the photocurrent J and electric field  $E: J \propto |E|^2$ . Figure 2(a) shows the calculated enhancement spectrum (black curve) and reflectivity spectrum (red dashed line) of a patch antenna array with the patch size  $s = 1.30 \mu\text{m}$  and period  $p = 8 \mu\text{m}$ . The two spectra show the same resonance at a wavelength of  $8.9 \mu\text{m}$ , indicating that the enhancement factor F plays the same role as the reflectivity in indicating the absorption ability of the structure. Moreover, the current responsivity of the detector is increased by the factor F. Here,  $F_{peak} = 600$ ; thus, the responsivity R is increased 600-fold. Figure 2(b) shows the calculated electric field enhancement  $F_{peak}$  (squares) as a function of the unit cell period p of the array. When the period p of the array is near or below the resonance wavelength, the coupling effect among these patches is dominant in enhancing the electric field, combined with the cavity effect. In contrast, when p is sufficiently large, the coupling effect can

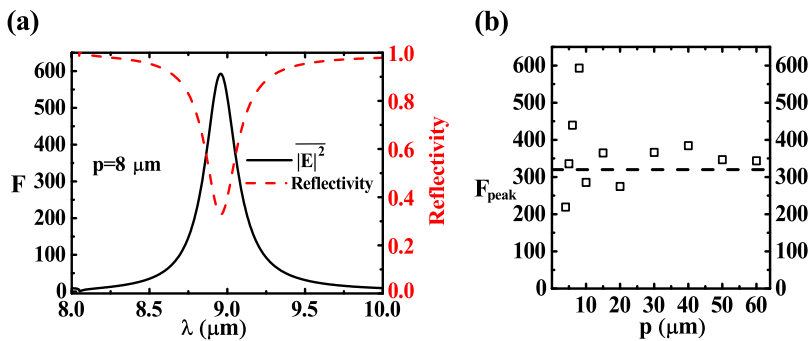


**FIG. 2.** Patch antenna array without gratings: (a) the calculated electric field enhancement spectrum (black curve) and reflectivity spectrum (red dashed line) of a patch antenna array, where the period p is  $8 \mu\text{m}$  and (b) the calculated electric field enhancement  $F_{peak}$  (squares) as a function of the unit cell period p of the array; The horizontal black dashed line indicates  $F_{peak} = 320$  for a single patch cavity (nonperiodic).

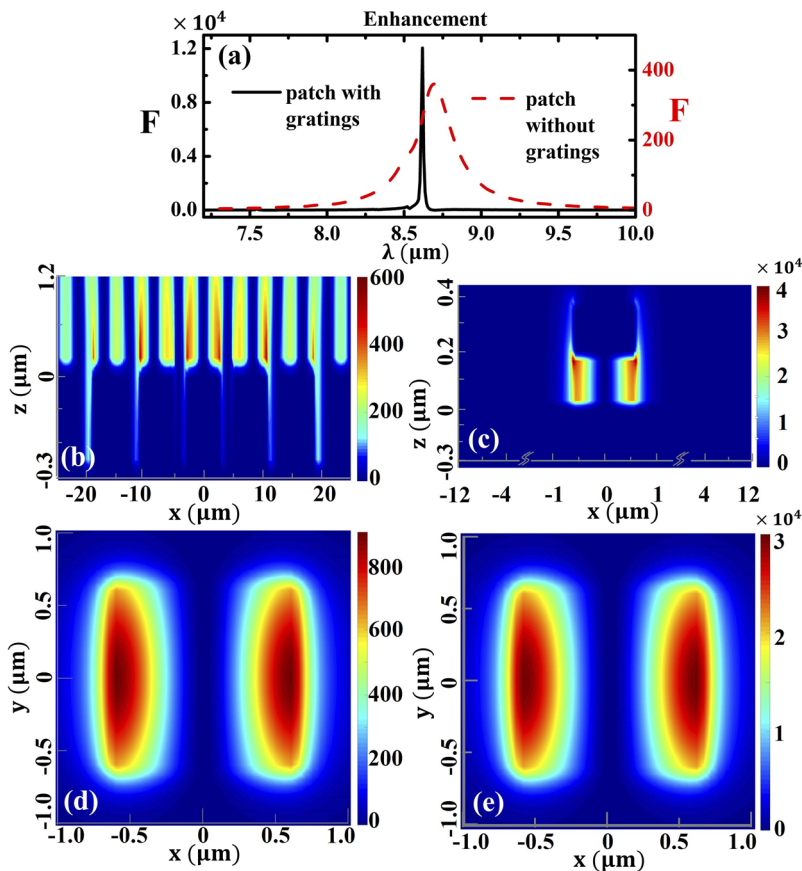


**FIG. 3.** (a) Calculated electric field enhancement spectra of a patch antenna array with gratings (black curve) and without gratings (red dashed line), [(b) and (c)] the calculated square of the intensity of the electric field distribution ( $|E|^2$ ) in the  $x$ - $z$  plane (plane  $y = 0 \mu\text{m}$ ) of the grating alone and the hybrid antenna at a wavelength of  $8.62 \mu\text{m}$ , and [(d) and (e)] calculated  $|E|^2$  inside the QW in the  $x$ - $y$  plane (plane  $z = 0.1 \mu\text{m}$ ) for a patch antenna array without or with gratings at wavelengths of  $8.69 \mu\text{m}$  and  $8.62 \mu\text{m}$ , respectively. The color bars indicate the ratios:  $\frac{|E_Q|^2}{E_0^2}$ .

be ignored, and the enhancement factor is simplified to the level of a single patch cavity.

Next, we combine the patch cavity with a grating, resulting in a hybrid antenna, to achieve a much larger intensity for the localized electric field. Figure 3(a) shows the calculated enhancement spectra of the hybrid antenna (black curve) and the patch antenna array (red dashed line) for comparison. The polarization of the incident light is about the  $x$  axis, and the primary parameters for this infrared antenna are listed in Table I ( $\lambda = 8.6 \mu\text{m}$ ). Clearly, the enhancement of the hybrid antenna is approximately a factor of 12 000 at the resonance wavelength of  $8.62 \mu\text{m}$ , which is much larger than that of the patch antenna array ( $\sim 350$ ). Briefly, this strong enhancement can be attributed to the coupling effect between the patch cavity mode and the grating mode.

Figure 3(b) shows the calculated square of the intensity of the electric field distribution ( $|E|^2$ ) in the  $x$ - $z$  plane (plane  $y = 0 \mu\text{m}$ ) for a solitary grating (without a patch cavity) at the resonance wavelength of  $8.62 \mu\text{m}$ . The electric field of the resonance mode of the grating is localized near the surface, and  $|E|^2$  reaches a maximum of  $\sim 600$ . When the mode of the grating matches that of the patch cavity or when the resonance wavelengths of the grating and cavity are similar (matching condition), the localized electric field is strongly enhanced. Figure 3(c) shows  $|E|^2$  in the  $x$ - $z$  plane (plane  $y = 0 \mu\text{m}$ ) for the hybrid antenna, in which the matching condition is satisfied.  $|E|^2$  reaches a maximum of  $\sim 40\,000$ . Figures 3(d) and 3(e) show  $|E|^2$  in the  $x$ - $y$  plane (plane  $z = 0.1 \mu\text{m}$ ) for the patch antenna array and the hybrid antenna at wavelengths of  $8.69 \mu\text{m}$  and  $8.62 \mu\text{m}$ , respectively. Obviously,

**TABLE I.** Primary parameters of the hybrid antennas: thickness of the Au layer  $H$ , unit period  $p$ , grating period  $g$ , depth  $h$ , width  $a$ , thickness of the QW and the metal  $t_Q$  and  $t_M$ , patch size  $s$ , and hold size  $s'$ . All values are given in  $\mu\text{m}$ . The indexes  $n_{QW}$  and  $n_{Au}$  indicate QW and Au, respectively.

Unit $\mu\text{m}$	$H$	$p$	$g$	$h$	$a$	$t_Q$	$t_M$	$s$	$s'$	$n_{QW}$	$n_{Au}$
$\lambda = 8.6$	2	60	8	0.3	6	0.2	0.2	1.25		3.4	$9.4 + 60i$
$\lambda = 100$	20	$10^3$	100	4	80	2	2	15	12	3.4	$225 + 319i$

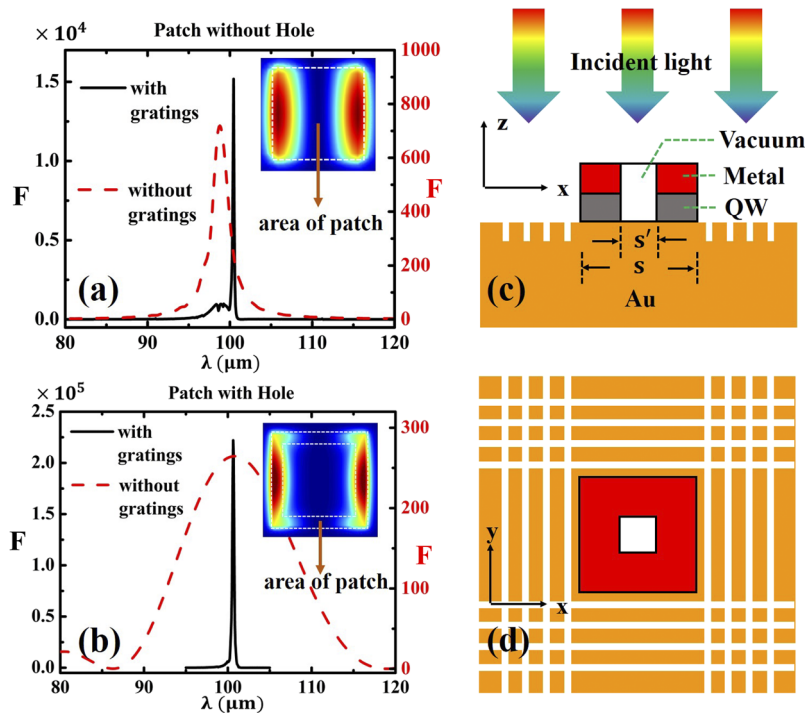


**FIG. 4.** Calculations for the THz frequency region: [(a) and (b)] the calculated electric field enhancement spectra for a patch antenna array with gratings (black curve) and without gratings (red dashed line) [(a) presents results for a structure without holes, while (b) displays results for the case with holes; the insets show the calculated  $|E|^2$  inside the QW in the  $x$ - $y$  plane (plane  $z = 1 \mu\text{m}$ ) for the hybrid antenna for a wavelength of  $100 \mu\text{m}$ ; the white dashed squares indicate the edges of the patch and the hole] and [(c) and (d)] the schematic of a unit cell of the modified hybrid antenna with a hole [(c) presents the  $x$ - $z$  plane view, and (d) presents the  $x$ - $y$  plane view; the patch schematic is magnified for enhanced clarity].

the enhancement factor is much larger for the hybrid antenna [Fig. 3(e)].

Thus far, we have performed calculations for a wavelength of  $\sim 9 \mu\text{m}$  and have obtained highly enhanced electric fields with an enhancement factor of up to 12 000, which is approximately 34-fold greater than that of the patch antenna array (350) and 12 000-fold greater than that under vacuum. Additionally, the resonance wavelength of the highly enhanced mode can be adjusted to other wavelength regions. As mentioned above, a highly enhanced mode occurs when the grating mode and patch cavity mode match. It is known that the resonance wavelength of the grating mode varies with the grating period  $g$ , and the resonance wavelength  $\lambda_{res}$  of the patch cavity follows  $\lambda_{res} = 2sn_{eff}$ ,<sup>10</sup> where  $s$  is the patch size, and  $n_{eff}$  is the effective index. Thus, we can adjust the enhanced mode to a desired wavelength by tuning the grating period and the size of the patch cavity. As an example, we calculated the results for two other cases (not shown).  $|E|^2$  inside the QW was highly enhanced at wavelengths of  $6.17 \mu\text{m}$  and  $10.07 \mu\text{m}$ , with enhancement factors of  $\sim 5500$  and  $\sim 15\,000$ , corresponding to the modes of hybrid antennas with grating periods of  $g = 6 \mu\text{m}$  and  $g = 10 \mu\text{m}$ , respectively. Here, the unit period was  $p = 60 \mu\text{m}$  for both cases.

In the THz region, the photon energy is low, which results in a very low SNR for the quantum well photodetector (QWP) at room temperature. Therefore, the QWP can only operate at very low temperatures ( $\sim 10 \text{ K}$ ),<sup>23</sup> which prevents its use in a broad range of applications. By employing the proposed structure, the resonance wavelength can be tuned over a wide range, rendering this design suitable not only for the infrared region but also for the THz region.

Figure 4(a) shows the calculated enhancement spectra for the hybrid antenna (black curve) and the patch antenna array (red

dashed line) for comparison. The parameters for this calculation are listed in Table I ( $\lambda = 100 \mu\text{m}$ ). The enhancement factor reaches 15 000 at a wavelength of  $\sim 100 \mu\text{m}$  ( $\sim 3 \text{ THz}$ ) for the hybrid antenna. The inset of Fig. 4(a) shows that the electric field is primarily localized near the edge rather than the center of the patch. Furthermore, the patch size ( $15 \mu\text{m}$ ) is sufficiently large to be etched experimentally. Hence, we modified our hybrid antenna by removing some material from the center of the patch, forming a square hole in the patch, i.e., making the patch into a square loop. As a result, the QW area and the dark current are reduced. Figures 4(c) and 4(d) show schematics of the modified hybrid antenna with a square hole, and the patch is magnified for enhanced clarity. The hole size is  $s' = 12 \mu\text{m}$ , and the patch size is  $s = 15 \mu\text{m}$ . The results for the modified structure are shown in Fig. 4(b), including the calculated enhancement spectra for the modified hybrid antenna (black curve) and the patch antenna array (red dashed line), both of which contain holes. There is almost no change in  $|E|^2$  in the inset of Fig. 4(b) compared with the inset of Fig. 4(a), which indicates the localization of the electric field. Here, an extremely high enhancement factor,  $F = 2.22 \times 10^5$ , is observed.

#### IV. DISCUSSION

The highly enhanced and localized electric field results in a strongly increased current responsivity  $R$ , which can increase the working temperature of the detector. For example, Palaferri *et al.* developed a device employing patch antennas,<sup>24</sup> with a responsivity  $R = 5.5 \text{ A/W}$ , photocurrent density  $J = 3.0 \times 10^{-4} \text{ A/cm}^2$ , and enhancement factor  $F = 150$  (we used our method to calculate this  $F$ )

at  $T = 4$  K. The typical dark current of a THz detector is approximately  $1.0 \times 10^{-4}$  A/cm<sup>2</sup> at  $T = 4$  K,<sup>23</sup> which allows their device to work well. With our enhancement factor reaching  $F' = 2.22 \times 10^5$  (THz), it can be estimated that  $R$  and  $J$  can be increased to  $R' = R \times F'/F = 8.14 \times 10^3$  A/W and  $J' = J \times F'/F = 4.44 \times 10^{-1}$  A/cm<sup>2</sup>. Thus, the dark current density should be smaller than  $J'$ , and from Ref. 23, we find that the temperature should be lower than 195 K. The improved  $R$  and  $J$  of our structure may enable the detection of THz radiation at a much higher temperature with QWPs.

Furthermore, we theoretically estimate the noise equivalent power (NEP) of our THz structure based on data from Palaferri *et al.*<sup>25</sup> We assume that our detector comprises  $N_P = 4 \times 4 = 16$  unit cells, corresponding to a material area of  $S_{QW} = N_P \times (s^2 - s'^2) = 1296 \mu\text{m}^2$ . Using the relationship between noise and the material area, the background current noise of our structure is estimated at approximately  $I_{N1} = S_{QW}/S_{Palaferri} \times I_{Palaferri} \approx 3.8 \times 10^{-14}$  A/Hz<sup>0.5</sup>, for  $T = 4$  K at a voltage of  $V = 50$  mV. Therefore, in this case,  $NEP_1 = I_{N1}/R' \approx 4.1 \times 10^{-18}$  W/Hz<sup>0.5</sup>. Next, according to the relationship between noise and temperature, we employ an Arrhenius plot to fit the noise-temperature curve (not shown) and obtain a noise value of  $I_{N2} \approx 4.4 \times 10^{-11}$  A/Hz<sup>0.5</sup> at room temperature,  $T = 300$  K, for a voltage of  $V = 50$  mV. In this case,  $NEP_2 = I_{N2}/R' \approx 5.4 \times 10^{-15}$  W/Hz<sup>0.5</sup>. At present, typical experimental NEP values are  $2.0 \times 10^{-13}$  W/Hz<sup>0.5</sup> at  $T = 4$  K<sup>25</sup> and  $2.0 \times 10^{-9}$  W/Hz<sup>0.5</sup> at room temperature.<sup>26</sup> These results can help improve the detectivity and working temperature of detectors while maintaining a sufficiently low NEP; for example, an acceptable value is estimated ( $10^{-15}$  W/Hz<sup>0.5</sup>) at room temperature.

Notably, some types of QWPs are only sensitive to the  $E_z$  component of an electric field. In this work, we also computed  $|E_z|^2$  compared with  $|E|^2$ . The former is 1.8% and 1.6% lower than the latter at 8.6  $\mu\text{m}$  and 100  $\mu\text{m}$  peaks, respectively. Thus, the main component of the electric field inside the QW is the  $E_z$  component, which is important for  $E_z$ -sensitive QWPs.

## V. CONCLUSIONS

In this study, we designed a hybrid antenna for midinfrared and THz photodetectors. Numerical simulations demonstrated that the hybrid antenna can effectively localize and strongly enhance the electric field inside the QW, with an enhancement factor exceeding  $10^5$ . The enhanced electric field inside the QW can greatly improve the performance of the detector. In the THz region, we theoretically estimate that our hybrid antenna can increase the working temperature up to 195 K. In addition, this antenna is theoretically expected to have a much lower NEP,  $10^{-18}$  W/Hz<sup>0.5</sup> at  $T = 4$  K (typical experimental data  $10^{-13}$  W/Hz<sup>0.5</sup>). Moreover, at room temperature,  $T = 300$  K, the estimated NEP is approximately  $10^{-15}$  W/Hz<sup>0.5</sup> (typical experiment data  $10^{-9}$  W/Hz<sup>0.5</sup>). These results can be applied to improve the performance of photodetectors operating over regions ranging from infrared to THz. Specially, for THz detectors, which generally operate at low temperature (4 K), these improvements can greatly increase their working temperature while

maintaining a low NEP. Thus, this approach may enable THz detection at room temperature.

## ACKNOWLEDGMENTS

This work was supported by the National Natural Science Foundation of China (NSAF) Joint Fund (Grant No. U1730246) and the National Natural Science Foundation of China (Grant No. F040302).

## REFERENCES

- D. Schurig, J. J. Mock, B. J. Justice, S. A. Cummer, J. B. Pendry, A. F. Starr, and D. R. Smith, *Science* **314**, 977 (2006).
- N. I. Landy, S. Sajuyigbe, J. J. Mock, D. R. Smith, and W. J. Padilla, *Phys. Rev. Lett.* **100**, 207402 (2008).
- H. Shen, G. Lu, T. Zhang, J. Liu, and Q. Gong, *Plasmonics* **8**, 869 (2013).
- H. Shen, G. Lu, T. Zhang, J. Liu, Y. He, Y. Wang, and Q. Gong, *J. Opt. Soc. Am. B* **30**, 2420 (2013).
- R. Y. Chou, G. Lu, H. Shen, Y. He, Y. Cheng, P. Perriat, M. Martini, O. Tillement, and Q. Gong, *J. Appl. Phys.* **115**, 244310 (2014).
- M. I. Stockman, *Phys. Rev. Lett.* **93**, 137404 (2004).
- N. Fang, H. Lee, C. Sun, and X. Zhang, *Science* **308**, 534 (2005).
- A. Kabashin, P. Evans, S. Pastkovsky, W. Hendren, G. Wurtz, R. Atkinson, R. Pollard, V. Podolskiy, and A. Zayats, *Nat. Mater.* **8**, 867 (2009).
- C. Watts, D. Shrekenhamer, J. Montoya, G. Lipworth, J. Hunt, T. Slesman, S. Krishna, D. Smith, and W. Padilla, *Nat. Photonics* **8**, 605 (2014).
- D. Palaferri, Y. Todorov, A. Bigioli, A. Mottaghizadeh, G. Djamal, A. Calabrese, A. Vasanelli, L. Li, A. Giles Davies, E. Linfield, F. Kapsalidis, M. Beck, J. Faist, and C. Sirtori, *Nature* **556**, 85 (2018).
- J. Li, C. Zhao, B. Liu, C. You, F. Chu, N. Tian, Y. Chen, S. Li, B. An, A. Cui, X. Zhang, H. Yan, D. Liu, and Y. Zhang, *Appl. Surf. Sci.* **473**, 633 (2019).
- B. F. Levine, K. K. Choi, C. G. Bethea, J. Walker, and R. J. Malik, *Appl. Phys. Lett.* **50**, 1092 (1987).
- H. C. Liu, R. Dudek, A. Shen, E. Dupont, C. Y. Song, Z. R. Wasilewski, and M. Buchanan, *Appl. Phys. Lett.* **79**, 4237 (2001).
- B. F. Jones, *IEEE Trans. Med. Imaging* **17**, 1019 (1998).
- Z. Liu, E. Blasch, Z. Xue, J. Zhao, R. Laganieri, and W. Wu, *IEEE Trans. Pattern Anal. Mach. Intell.* **34**, 94 (2012).
- X. Qian, X.-H. Peng, D. O. Ansari, Q. Yin-Goen, G. Chen, D. Shin, L. Yang, A. Young, M. Wang, and S. Nie, *Nat. Biotechnol.* **26**, 83 (2008).
- A. Rogalski, *Prog. Quantum Electron.* **27**, 59 (2003).
- F. Schuster, D. Coquillat, H. Videlier, M. Sakowicz, F. Teppe, L. Dussopt, B. Giffard, T. Skotnicki, and W. Knap, *Opt. Express* **19**, 7827 (2011).
- N. Youngblood, C. Chen, S. J. Koester, and M. Li, *Nat. Photonics* **9**, 247–252 (2015).
- M. A. Ordal, R. J. Bell, R. W. Alexander, L. L. Long, and M. R. Querry, *Appl. Opt.* **26**, 744 (1987).
- R. T. Holm, J. W. Gibson, and E. D. Palik, *J. Appl. Phys.* **48**, 212 (1977).
- J. Y. Andersson and L. Lundqvist, *J. Appl. Phys.* **71**, 3600 (1992).
- M. Graf, G. Scalari, D. Hofstetter, J. Faist, H. Beere, E. Linfield, D. Ritchie, and G. Davies, *Appl. Phys. Lett.* **84**, 475 (2004).
- D. Palaferri, Y. Todorov, Y. N. Chen, J. Madeo, A. Vasanelli, L. H. Li, A. G. Davies, E. H. Linfield, and C. Sirtori, *Appl. Phys. Lett.* **106**, 161102 (2015).
- D. Palaferri, Y. Todorov, D. Gacemi, S. Barbieri, L. H. Li, A. G. Davies, E. H. Linfield, and C. Sirtori, *Appl. Phys. Lett.* **113**, 161105 (2018).
- M. Vitiello, D. Coquillat, L. Viti, D. Ercolani, F. Teppe, A. Pitanti, F. Beltram, L. Sorba, W. Knap, and A. Tredicucci, *Nano Lett.* **12**, 96 (2011).